

Supplementary information for:
Tropical cloud feedbacks estimated from observed multi-decadal
trends

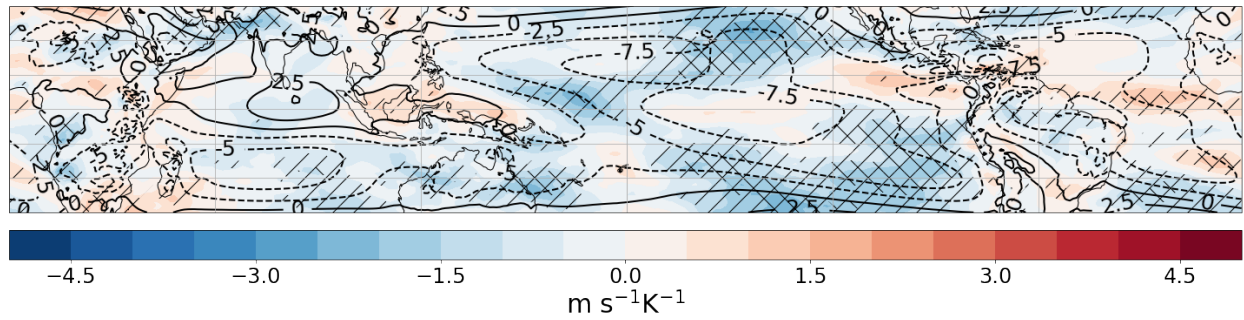
Emily K. Van de Koot^a, Michael P. Byrne^b, Tim Woollings^a

^a *Atmospheric, Oceanic and Planetary Physics, University of Oxford,
Oxford, United Kingdom*

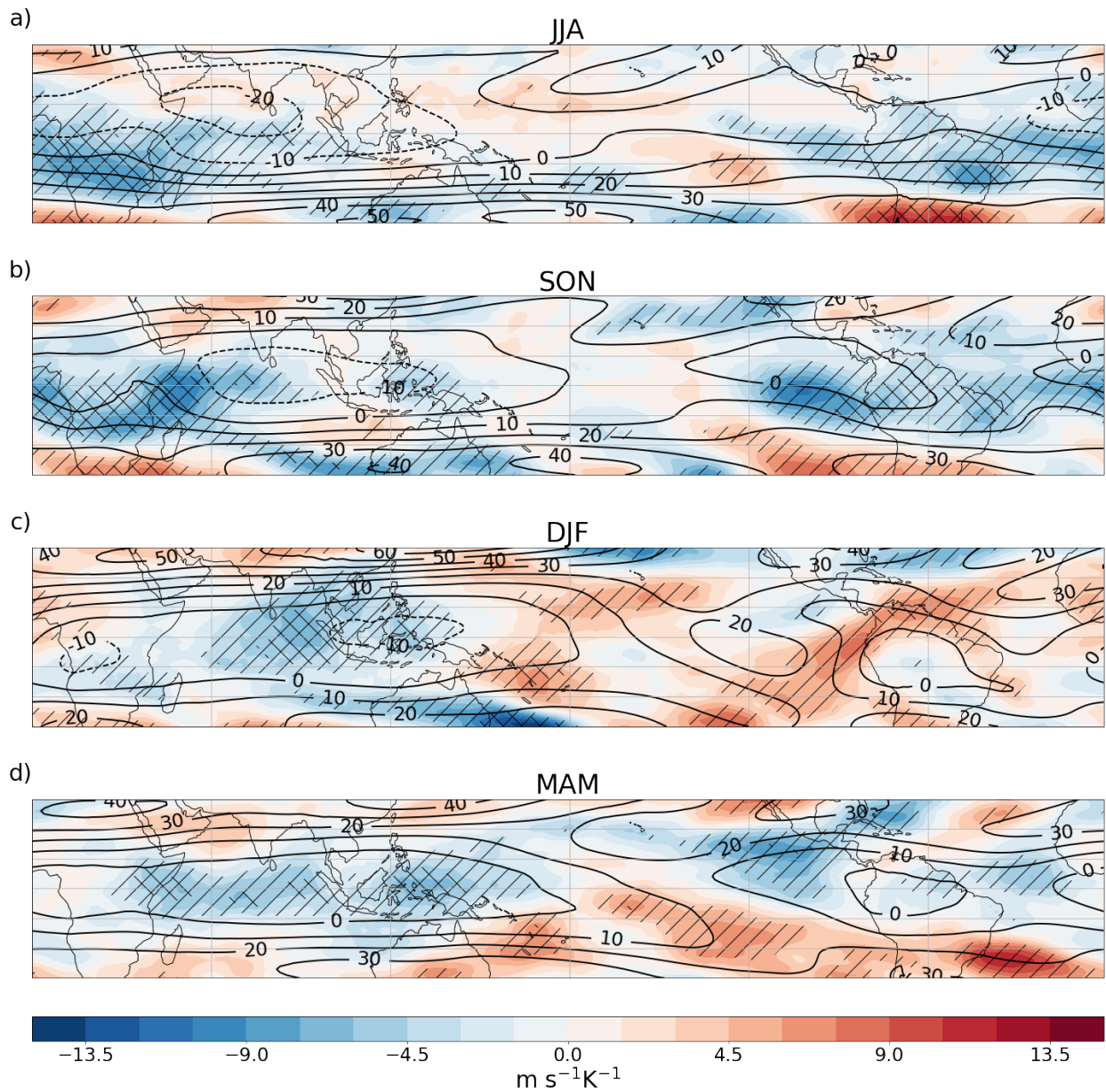
^b *School of Earth and Environmental Sciences, University of St Andrews,
St Andrews, United Kingdom*

March 6, 2025

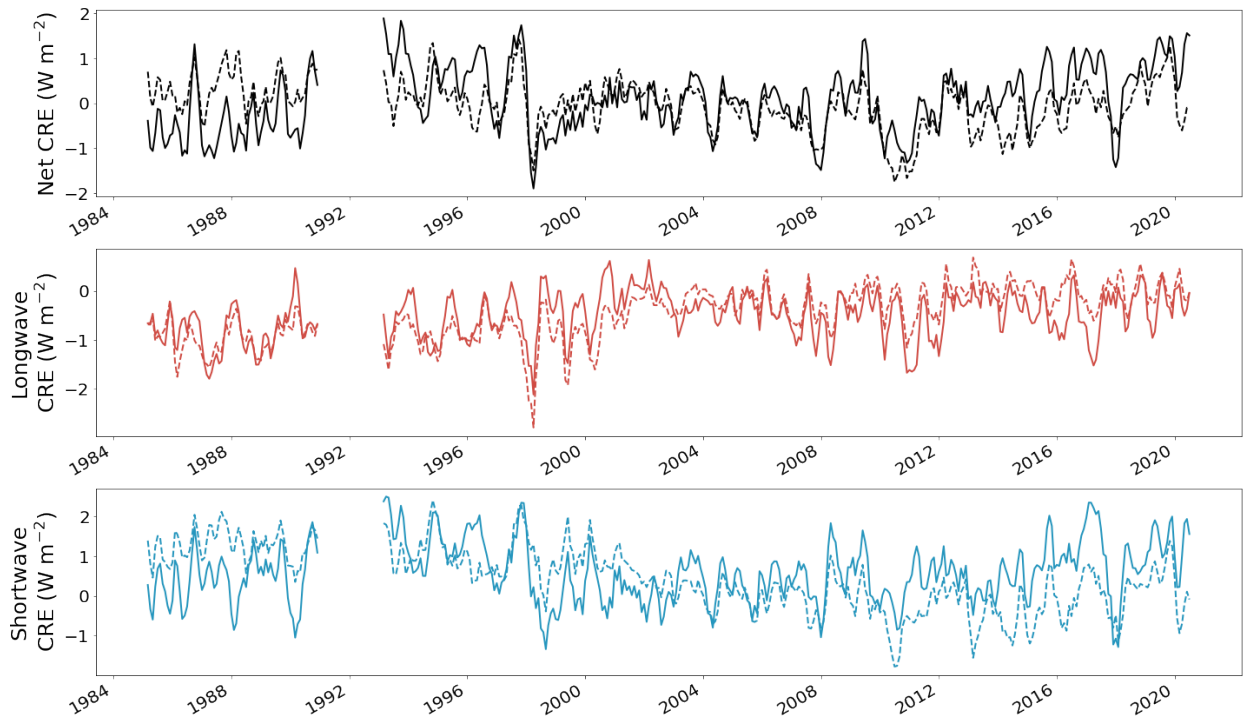
1 Supplementary figures



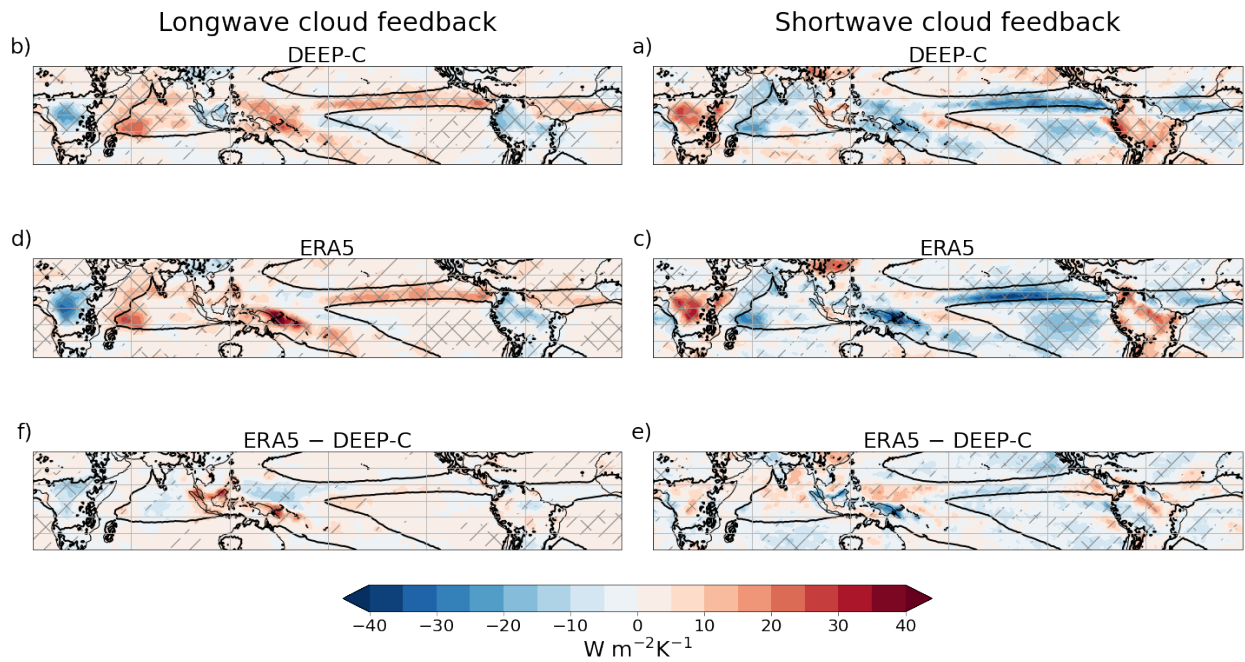
Supplemental Figure 1: Changes in eastward wind at 850 hPa per degree tropical warming calculated from trends between 1985 and 2020. Regions where the magnitude of the sensitivity to warming is larger than the standard error are hatched and regions where it is larger than twice the standard error are cross-hatched. Black contours show the climatology.



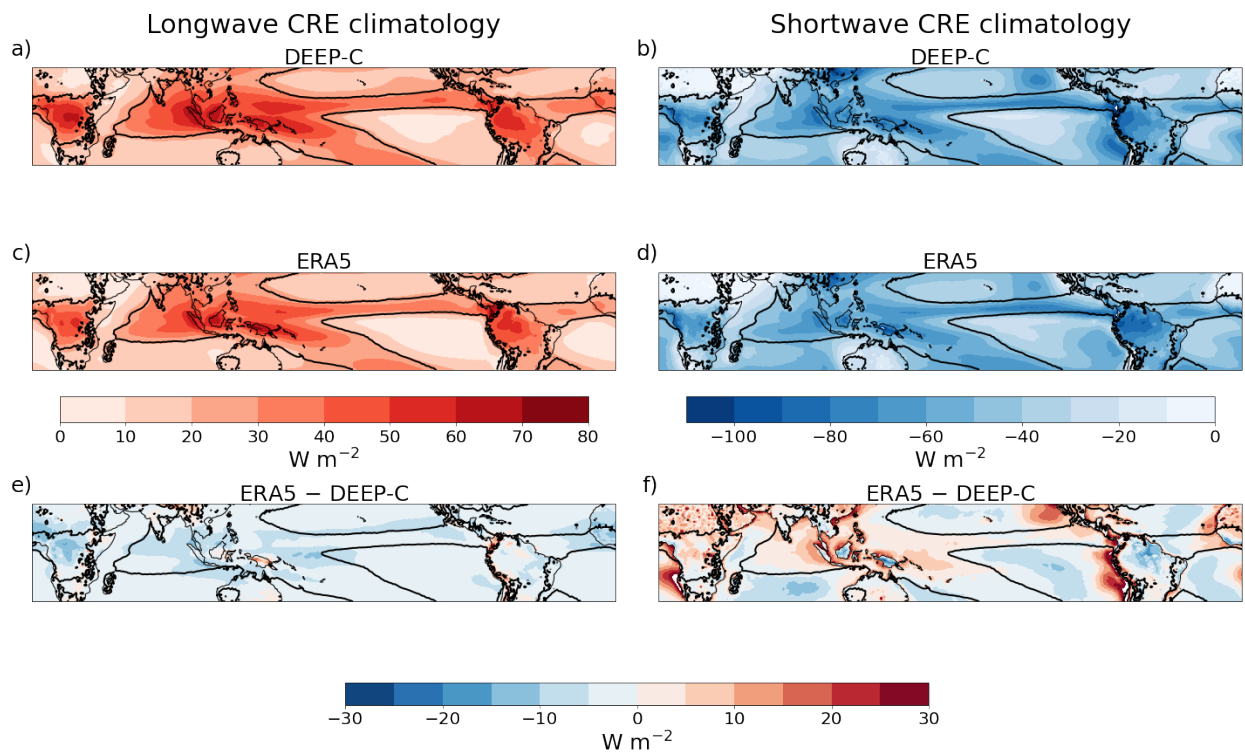
Supplemental Figure 2: Changes in eastward wind at 200 hPa per degree tropical warming calculated from trends between 1985 and 2020 averaged over (a) June-August, (b) September-November, (c) December-February and (d) March-May. Regions where the magnitude of the sensitivity to warming is larger than the standard error are hatched and regions where it is larger than twice the standard error are cross-hatched. Black contours show the climatology.



Supplemental Figure 3: DEEP-C (solid lines) and ERA5 (dashed lines) estimates of the (a) net, (b) longwave and (c) shortwave kernel-adjusted deseasonalised CRE anomalies between 1985 and 2020 averaged over tropical descending regions (i.e. where $\omega > 0$ hPa day⁻¹) only. Years 1991 – 1992 are excluded due to the effect of volcanic aerosol from the Pinatubo eruption on TOA fluxes. To allow comparison with Liu et al. (2020) Figure 1, anomalies are taken relative to the 2001 – 2005 climatology and a three-month running mean is applied.



Supplemental Figure 4: The longwave and shortwave cloud feedbacks calculated from trends between 1985 and 2020 estimated by (a,c) DEEP-C and (b,d) ERA5. Panels (e) and (f) show the differences between the datasets for the longwave and shortwave feedbacks, respectively. Regions where the magnitude of the feedback is larger than the standard error are hatched and regions where it is larger than twice the standard error are cross-hatched. The black contour divides regions of climatological ascent and descent.



Supplemental Figure 5: The longwave and shortwave CRE climatology over 1985 to 2020 estimated by (a,c) DEEP-C and (b,d) ERA5. Panels (e) and (f) show the differences between the datasets for the longwave and shortwave climatologies, respectively. The black contour divides regions of climatological ascent and descent.

2 Supplementary Tables

		DEEP-C		ERA5	
		CRE in ω -regimes	Tropical-mean CRE	CRE in ω -regimes	Tropical-mean CRE
Tropical-mean cloud feedback ($\text{W m}^{-2}\text{K}^{-1}$)	Net	0.22 (0.23)	0.31 (0.27)	-1.33 (0.23)	-1.22 (0.22)
	LW	1.42 (0.22)	1.78 (0.20)	1.99 (0.19)	2.26 (0.18)
	SW	-1.20 (0.37)	-1.47 (0.34)	-3.32 (0.36)	-3.48 (0.31)

Supplemental Table 1: Net, longwave (LW) and shortwave (SW) tropical-mean cloud feedbacks estimated from trends between January 1985 and July 2020 using DEEP-C and ERA5. Feedbacks denoted ‘CRE in ω -regimes’ are calculated following equation 2. Feedbacks denoted ‘Tropical-mean CRE’ are calculated by finding the trend in monthly-mean tropical-mean CRE anomalies, dividing this by the trend in the monthly-mean tropical-mean surface temperature anomalies, and then taking the average over months. Errors are the standard error (1σ) of the regression error only (i.e. do not include instrument error) to allow comparison of calculation methods.

Dataset	All-sky	DEEP-C	CERES-EBAF	CERES-EBAF	ERA5
	Clear-sky	ERA5	ERA5	CERES-EBAF	ERA5
Tropical-mean cloud feedback ($\text{W m}^{-2}\text{K}^{-1}$)	Net	2.22 (0.39)	2.22 (0.39)	-0.34 (0.33)	0.75 (0.39)
	LW	-0.51 (0.37)	-0.52 (0.36)	-2.27 (0.37)	0.81 (0.31)
	SW	2.73 (0.63)	2.74 (0.62)	1.92 (0.58)	-0.06 (0.60)

Supplemental Table 2: Net, longwave (LW) and shortwave (SW) tropical-mean cloud feedbacks estimated from trends between March 2000 and July 2020 following equation 2. CERES-EBAF Ed. 4.1 (NASA/LARC/SD/ASDC, 2019) is used. The CERES-EBAF clear-sky data is type ”t”, i.e., it is for the total region, not just clear portions. Errors are the combined regression and instrument standard error (1σ) to allow comparison of datasets.

3 Estimation of DEEP-C instrument uncertainty

Liu et al. (2020) estimate the uncertainty on the global- and annual-mean net radiative flux change between 1985 – 2000 to be $\pm 0.61 \text{ W m}^{-2}$ at the 90% confidence level. This uncertainty is associated with gaps in the observational record in 1993 and 1999 – 2000. Johnson et al. (2016) estimate the uncertainty on the change in radiative flux over the CERES period (2000 – 2020) to be $\pm 0.10 \text{ W m}^{-2}$, also at 90% confidence level. Uncertainty on the CERES data is based on uncertainty on ocean heat uptake measured by Argo (Roemmich and Argo Steering Team, 2009), which is used to validate and anchor the satellite data (Loeb et al., 2012).

To estimate the instrument uncertainty on the cloud feedback, we begin by estimating the uncertainty on the change in net all-sky radiative flux to be $\sqrt{(0.61)^2 + (0.10)^2} = 0.62 \text{ W m}^{-2}$. Assuming no instrument uncertainty on the ERA5-derived clear-sky fluxes, the instrument uncertainty on the change in CRE is also 0.62 W m^{-2} . To convert to an error on the feedback, we divide by the number of years and then by the tropical-mean surface temperature trend over the same period, producing an error of $1.09 \text{ W m}^{-2}\text{K}^{-1}$. Assuming that the data are normally distributed, we convert this to a standard error (1σ) of $0.66 \text{ W m}^{-2}\text{K}^{-1}$. We assume that this error is independent of the area it covers as it depends on global factors that affect the satellite calibration equally in all regions.

Consequently, we add (in quadrature) an instrument error of $0.66 \text{ W m}^{-2}\text{K}^{-1}$ to the existing error on the linear regression for feedbacks associated with individual vertical velocity regimes (e.g., Fig 2d,e)

or gridpoints (e.g., Fig. 5a-c). We add (in quadrature) an instrument error of $0.66 \text{ W m}^{-2}\text{K}^{-1} \times P(\omega)$ to the non-dynamic component of the contribution of each vertical velocity regime to tropical-mean cloud feedbacks and an instrument error of $0.66 \text{ W m}^{-2}\text{K}^{-1} \times (dP(\omega)/d\bar{T})$ to the nonlinear component (e.g., Fig 4). To calculate the instrument error on tropical-mean feedback values we sum (*not* in quadrature) the thermodynamic and nonlinear component instrument errors over vertical velocity regimes and then add together (in quadrature) the totals of these sums. This leads to an instrument error marginally larger than $0.66 \text{ W m}^{-2}\text{K}^{-1}$ because we use $d\text{CRE}(\omega)/d\bar{T}$ twice in our calculation method. Note that we would expect the total thermodynamic and nonlinear component instrument errors to be related but, for simplicity, we add them in quadrature. This decision has limited impact because the instrument error on the nonlinear component is much smaller than that on the thermodynamic component. Also note that (in contrast to the instrument errors) we sum the linear regression errors over vertical velocity regimes in quadrature. To calculate the overall error on tropical-mean feedback values we add the tropical-mean regression error and the tropical-mean instrument error in quadrature.

4 Estimation of global anvil area and albedo feedback

We begin by estimating the contribution to the net tropical-ocean-mean cloud feedback from deep convective regions for DEEP-C. The method is as outlined in sections 3 but the analysis is performed over tropical oceans only, the global mean (rather than tropical-mean) temperature time-series is used for consistency with Sherwood et al. (2020), and we only integrate over vertical velocity regimes with $\omega < 0 \text{ hPa day}^{-1}$ to isolate the contribution of ascending regions. Results are shown in table 3. For the trend-derived overall and non-dynamic feedback estimates, the instrument error is $0.19 \text{ W m}^{-2}\text{K}^{-1}$ (1σ). There are two reasons why the instrument error is lower for these estimates than for the tropical-mean cloud feedback estimates discussed in section 4. First, the instrument error depends inversely on the temperature trend and the global mean temperature trend exceeds the tropical mean temperature trend. Second, we scale the tropical-ocean-mean instrument error by the ratio of the area of ascent over tropical oceans to the total tropical ocean area to find the contribution to the tropical-ocean-mean instrument error from regions of oceanic ascent. Note that the regression errors are also reduced relative to the tropical-mean case. This is because, to study ascending regions only, we consider fewer vertical velocity regimes meaning fewer individual regression errors are combined to form the overall regression error. Recall that to calculate the combined instrument and regression errors we sum the 1σ errors in quadrature and then multiply by two.

		Feedback ($\text{W m}^{-2}\text{K}^{-1}$)
Trend-derived	Total	-0.54 (0.42)
	Non-dynamic	-0.60 (0.38)
Variability-derived	Total	-0.20 (0.33)

Supplemental Table 3: The contribution to the net tropical-ocean-mean cloud feedback from deep convective regions estimated from trends and detrended inter-annual variability between 1985 and 2020 using DEEP-C. Errors are twice the combined regression and instrument standard error.

To convert into an estimate of the global anvil area and albedo feedback, we first remove the cloud altitude feedback, estimated to be $0.40 \text{ W m}^{-2}\text{K}^{-1}$ locally following Sherwood et al. (2020). We scale this by the ratio of the area of ascent over tropical oceans to the total tropical ocean area to find the contribution to the tropical-ocean-mean feedback ($0.15 \text{ W m}^{-2}\text{K}^{-1}$). We assume there is no error on the altitude feedback estimate. Second, we convert from a tropical-ocean-wide anvil area and albedo feedback to a global-mean feedback by scaling the feedback estimate and the associated error by the fraction of the earth covered by tropical ocean.

References

- Johnson, G. C., J. M. Lyman, and N. G. Loeb, 2016: Improving estimates of Earth’s energy imbalance. *Nat. Clim. Change*, **6** (7), 639–640.
- Liu, C., and Coauthors, 2020: Variability in the global energy budget and transports 1985–2017. *Climate Dyn.*, **55**, 3381–3396.
- Loeb, N. G., J. M. Lyman, G. C. Johnson, R. P. Allan, D. R. Doelling, T. Wong, B. J. Soden, and G. L. Stephens, 2012: Observed changes in top-of-the-atmosphere radiation and upper-ocean heating consistent within uncertainty. *Nat. Geosci.*, **5** (2), 110–113.
- NASA/LARC/SD/ASDC, 2019: CERES Energy Balanced and Filled (EBAF) TOA and Surface Monthly means data in netCDF Edition 4.1. NASA Langley Atmospheric Science Data Center DAAC, URL https://doi.org/10.5067/TERRA-AQUA/CERES/EBAF_L3B.004.1.
- Roemmich, D., and Argo Steering Team, 2009: Argo: the challenge of continuing 10 years of progress. *Oceanography*, **22** (3), 46–55.
- Sherwood, S. C., and Coauthors, 2020: An assessment of Earth’s climate sensitivity using multiple lines of evidence. *Rev. Geophys.*, **58** (4), e2019RG000678.